ISSN 0208-7774 TRIBOLOGIA 3/2021 p. 9–18
DOI: 10.5604/01.3001.0015.6892

Tomasz DESANIUK[*], Dominika SOBOŃ[**], Wojciech JURCZAK[***]

EFFECT OF HUMIDITY ON TRIBOLOGICAL PROPERTIES OF SELECTED FRICTION JUNCTIONS WITH AN EVALUATION OF ACOUSTIC EMISSION

WPŁYW WILGOTNOŚCI NA WŁAŚCIWOŚCI TRIBOLOGICZNE WYBRANYCH WĘZŁÓW TARCIA WRAZ Z OCENĄ EMISJI AKUSTYCZNEJ

Key words: friction, humidity, wear, acoustic emission, ball-on-disc.

Abstract: The study aimed to compare the effect of humidity on the operation of tribological systems. The tested friction and wear are external properties; therefore, their values may differ significantly depending on the operating parameters of the friction junction and environmental conditions. Tribological tests were carried out on a TRB^3 tribometer in a dry sliding mode at a relative humidity of 50% ± 5% and 90% ± 5% in the ball-on-disc configuration with a load of 15 N. The friction junction consisted of a sample made of 100Cr6 steel, and three counter-samples were made of 100Cr6, SiC, and Al_2O_3 steel. The geometric structure of the surface was examined with an optical profiler. The tribological test results showed reduced linear wear and friction coefficient at a relative humidity of 90% ± 5% compare to its 50% ± 5%. The paper also presents the results for the sound recorded in the 16-bit linear PCM standard and analysed in a Spectra-Plus program.

Słowa kluczowe: tarcie, wilgotność, zużycie, emisja akustyczna, kula–tarcza.

Streszczenie: Celem badania było porównanie wpływu wilgotności na działanie systemów tribologicznych. Badane tarcie i zużycie są właściwościami zewnętrznymi, dlatego ich wartości mogą się znacząco różnic w zależności od parametrów pracy węzła tarcia i warunków otoczenia. Testy tribologiczne zostały przeprowadzone na tribometrze TRB^3 w warunkach tarcia technicznie suchego w ruchu ślizgowym przy względnej wilgotności 50% ± 5% i 90% ± 5%. Testy wykonano w skojarzeniu trącym kula–tarcza, gdzie węzeł tarcia stanowiła próbka wykonana ze stali 100Cr6 oraz trzy przeciwpróbki wykonane ze stali 100Cr6, SiC oraz Al_2O_3. Testy przeprowadzono dla obciążenia 15 N. Badania struktury geometrycznej powierzchni wykonano profilometrem optycznym. Przeprowadzone testy tribologiczne wykazały mniejsze zużycie liniowe oraz mniejszy współczynnik tarcia przy względnej wilgotności 90% ± 5%. W pracy przedstawiono również analizę dźwięku zarejestrowanego w standardzie 16-bitowego liniowego PCM, a następnie poddano go analizie w programie Spectra-Plus.

INTRODUCTION

The work of a tribological system consists of providing the necessary amount of energy to overcome the resistance resulting from the processes that accompany friction. As a result of friction, the energy is transformed into other forms of energy: thermal, electrical, and mechanical. The forms of energy that occur during friction are shown in **Figure 1**. The energy-triggered tribochemical reactions play a key role in the transformation of a surface layer into the layer with desirable functional properties that are suitable for specified technological applications **[L. 1**, **2]**.

[*] ORCID: 0000-0002-1565-423X. Kielce University of Technology, Faculty of Mechatronics and Mechanical Engineering, Tysiąclecia P.P. 7 Ave, 25-314 Kielce, Poland.
[**] ORCID: 0000-0001-7697-6884. Kielce University of Technology, Faculty of Mechatronics and Mechanical Engineering, Tysiąclecia P.P. 7 Ave, 25-314 Kielce, Poland.
[***] ORCID: 0000-0002-1608-7249. Polish Naval Academy, Faculty of Mechanical and Electrical Engineering, St. Jana Śmidowicza 69 Street, 81-127 Gdynia, Poland.

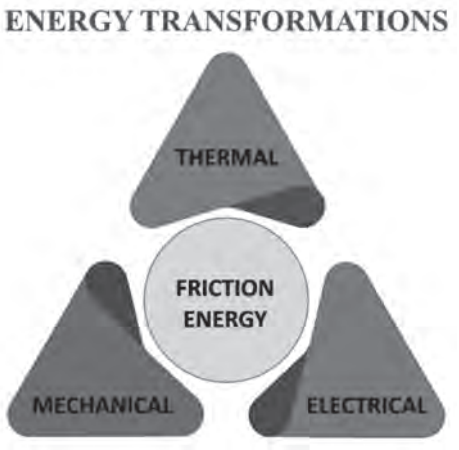

Fig. 1. Forms of energy occurring during friction in tribological systems [L. 1–2]

Rys. 1. Formy energii występujące podczas tarcia w systemach tribologicznych **[L. 1–2]**

Friction implies material losses and energy consumption. To mitigate these phenomena, it is necessary to take into account the conditions of close and distant environments in tribological processes. These include contact pressure, sliding speed, material type, and environmental factors, such as temperature, humidity, and atmosphere composition. In the case of humidity, water absorption is invisible, and the reaction between the water and tribological materials occurs only in the contact zone at ambient temperature. Water molecules between sliding surfaces act as a lubricant. Friction and wear levels vary depending on the material used and the level of humidity. Tribological tests demonstrate that friction and wear decrease with increasing humidity **[L. 3].**

High hardness and mechanical strength of advanced structural ceramics with Al_2O_3 ionic bonding and covalent SiC bonding make them suitable as tribological materials **[L. 4–8].** The wear of ceramic materials is classified into three categories: (I) mechanical fracture under high stress, (II) third body abrasion induced by abrasive debris, and (III) material removal due to tribochemical reactions **[L. 5]**. When tested for the effect of surface moisture on their tribological properties in unlubricated conditions, friction and wear decrease with increasing humidity **[L. 3**, **9–11]**. Experiments have shown **[L. 3]** that, in low humidity conditions, the test surface is rough; whereas, under high humidity, it is relatively smoother due to adsorbed water molecules. Hydroxides formed as a main product of ceramic tribology are considered lubricating and can have a protective function that prevents further wear of the substrate. The surface of the ceramics in a humid environment can increase the adhesion between the worn particles **[L. 12]**, which improves the lubricating ability between the friction junctions.

When steel surfaces are used, the friction and wear usually decrease with increasing humidity **[L. 13–14]**. In the intermediate area (45 ~ 65% RH), the friction coefficient decreases. Z. Chen **[L. 3]**, Y. Wang **[L. 15]** and other researchers suggest that water allows the formation of oxide layers on worn steel surfaces, and thus reduces the adhesive wear and friction force. The surfaces produced in this way commonly show good adhesion, which results in an increase in the friction force **[L. 16].**

In tribological processes, friction and wear performance in humid environments is not determined by the mechanical properties of the abraded materials. The water molecules at the surface subjected to abrasion in the tribological system are important. Products resulting from the interaction between water and the materials used in the tribological friction junction usually act as a protective film, reducing friction and wear **[L. 3].**

Acoustic emission (AE), which enables the study of the onset of the slip, is an important technique used to describe the friction process. This technology involves the generation and propagation of elastic waves in the range from 100 to 1000 kHz originating from a rapid release of elastic energy in the material as a result of structural changes that occur due to mechanical or thermal stresses **[L. 17–19]**. Waves can originate in processes such as particle dislocation, cracking, or stick-slip.

An AE test during tribological tests can identify the processes and changes to those processes. Part of the released frictional energy disperses in the form of elastic waves, which causes their propagation in the material, depending on its geometry and elastic properties **[L. 17, 20]**. The relationship between the wear rate and AE can be used for the identification of various damage types **[L. 17, 21]**. The correlations between AE amplitudes and friction are not universal. Acoustic emission levels alone are not sufficient for the correct the determination of wear **[L. 25]**. Due to the complexity of wear processes, finding an unambiguous relationship between wear and AE is problematic **[L. 17, 26]**.

The article compares the results of friction, linear wear, and surface geometry with tests carried out on the 100Cr6-100Cr6, 100Cr6-Al_2O_3, and 100Cr6-SiC configurations. The original

research that analysed the sound generated during the operation of the tribological system was also presented. All experiments were carried out under conditions of dry sliding friction at a relative humidity of 50% ± 5; 90% ± 5%, and a load of 15 N.

MATERIALS AND TEST METHODOLOGY

Tribological tests were performed on an Anton Paar TRB^3 ball-on-disc tribometer in a dry sliding mode. A photograph of the tester and a diagram of the friction junction are shown in **Fig. 2**. **Table 1** compiles the process and environmental parameters used. The tests were carried out with a load of 15 N for a relative humidity of 50% ± 5% and 90% ± 5%.

100Cr6 discs 42 mm in diameter with a height of 6 mm were the test samples. The chemical composition of the test material is given in **Table 2.**

Table 3 compiles the most important mechanical properties of 100Cr6 steel.

The balls with a diameter of 6 mm were made of 100Cr6 steel, silicon carbide – SiC, and aluminium (III) oxide – Al_2O_3.

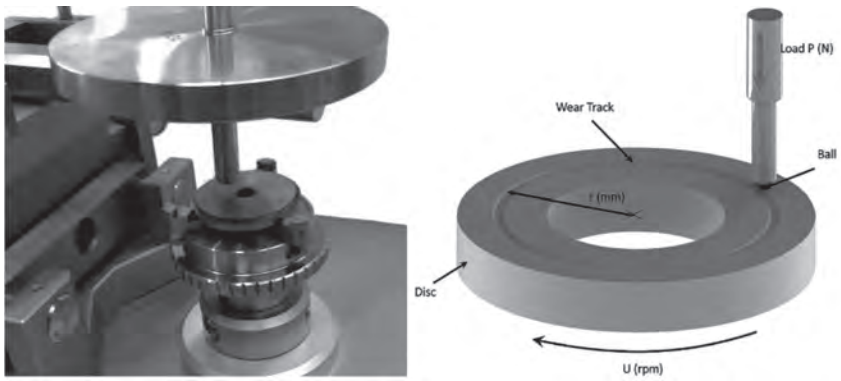

Fig. 2. Anton Paar TRB3 tribometer (a), ball-on-disc diagram (b) [L. 2]
Rys. 2. Tribometr Anton Paar TRB3 (a), schemat węzła tarciowego typu ball-on-disc (b) **[L. 2]**

Table 1. Test parameters
Tabela 1. Parametry badania

Parameter	Unit	Value
Load	N	15
Sliding rate	m/s	0.07
Number of cycles	–	1000
Humidity	%	50 ± 5; 90 ± 5
Temperature	°C	25 ± 1
Radius	mm	12

Table 2. Chemical structure of 100Cr6 steel discs
Tabela 2. Skład chemiczny krążków ze stali 100Cr6

Element									
C	**Si**	**Mn**	**P**	**S**	**Cr**	**Mo**	**Cu**	**Al**	**O**
0.93–1.05	0.15–0.35	0.25–0.45	max. 0.025	max. 0.015	1.35–1.60	max. 0.10	max. 0.30	max. 0.050	max. 0.0015

Table 3. Mechanical properties of 100Cr6 steel [L. 2, 27]
Tabela 3. Właściwości mechaniczne stali 100Cr6 **[L. 2, 27]**

Material	Young's modulus E [GPa]	Tensile strength R_m [MPa]	Compressive strength [MPa]	Hardness [Vickers]	Density [g/cm^3]
steel 100Cr6	243	520	454	210	7.83

The combination of ball-on-disc configurations is shown in **Table 4**. Test 1 was performed for a 100Cr6 steel disc and ball, Test 2 was performed for a 100Cr6 steel disc and an Al_2O_3 ball, and Test 3 was performed for a 100Cr6 steel disc and a SiC ball.

Table 4. Ball-on-disc tests configuration
Tabela 4. Skojarzenia trące kula–tarcza

Test	Disc	Ball
Test 1	100Cr6 steel	100Cr6 steel
Test 2	100Cr6 steel	Al_2O_3
Test 3	100Cr6 steel	SiC

Geometric structure was evaluated using a Leica DCM8 optical profiler in an interferometry mode. During the tests, the sound was recorded using an OLYMPUS PCM RECORDER LS-P1. The A-weighted equivalent sound levels were recorded in 0.1 second intervals with a Svan 971 Class 1 sound level meter. In the next step, the A-weighted equivalent sound level was determined for a 10-second time segment, using the following formula (1):

$$L_{Aeq} = 10log\left(\frac{1}{N}\sum_{i=1}^{N}10^{0.1L_{A,i}}\right), \quad (1)$$

where $L_{A,i}$ is the A – weighted equivalent continuous sound level in the *i*-th 0.1 – second time interval, and N = 100 is the number of 0.1 – second time intervals within 10 seconds.

A Sensirion SHT31 sensor was used to measure humidity. This sensor has a typical accuracy of ±2%RH and ±0.3°C and was factory calibrated. It was connected to an Arduino Leonardo through a digital I2C communication interface. To control humidity, an ultrasonic humidifier and a dehumidifier, based on a Peltier cell module, were used. The control program read the humidity from the sensor and turned on the humidifier to achieve the set humidity. The dehumidifier was switched on manually when there was a need for lower humidity than in the laboratory. The air temperature was controlled by the laboratory air conditioner, when it reached the set temperature, the hermetic cover of the tribometer was closed, and the Arduino program started to control the humidity.

RESULTS AND DISCUSSION

The performed tests aimed to compare the influence of the relative humidity conditions on the operation of the tribological system and the selected materials. In order to assess the surface damage after the tests, the geometric structure of the wear tracks was analysed and their maximum depth and wear area were determined. **Figure 3** shows isometric view images and initial surface profiles of the discs before (**Fig. 3a**) and after (**Fig. 3b–g**) tribological tests. Comparison of the results revealed the smallest signs of wear for the 100Cr6 – SiC pair (at a relative humidity of 50% ± 5%, the maximum depth was 3.087 μm, and the maximum width was about 0.35 mm. At a relative humidity of 90% ± 5%, the maximum depth was 4.264 μm, and the width was about 0.7 mm). On the other hand, the deepest trace of wear was observed for the 100Cr6 steel – Al_2O_3 pair (at a relative humidity of 50% ± 5% – the maximum depth was 92.81 μm, and a width of about 0.83 mm; at a relative humidity of 90% ± 5% – the maximum depth was 30.1 μm, a width of about 0.55 mm). Analysis of the obtained images and surface profiles indicated that the wear area decreased with increasing humidity conditions. Higher humidity has a positive effect on the performance of tribological systems.

Table 5 compiles the disc geometric structure parameters after tribological testing. Assessment of the surface geometric structure parameters, Sa (arithmetic average of the absolute surface heights), Sq (root mean square value of surface ordinates), Sp (maximum peak height), Sz (maximum surface height), Sku (flatness of the height distribution curve or kurtosis), Sv (maximum valley depth), and Ssk (the symmetry of height distribution about the mean plane), revealed the highest values for the 100Cr6 – Al_2O_3 sliding pair and the lowest values for the 100Cr6 – SiC configuration. Similarly to the interpretation results for the isometric view images of original surface profiles, the parameters of the geometric structure decrease with increasing relative humidity conditions.

Figure 4 shows the coefficient of friction (**Fig. 4a, 4b**) and linear wear (**Fig. 4c, 4d**) as a function of sliding distance for tribological tests and the sound level (**Fig. 4e, 4f**) for sliding surfaces in **Table 4**.

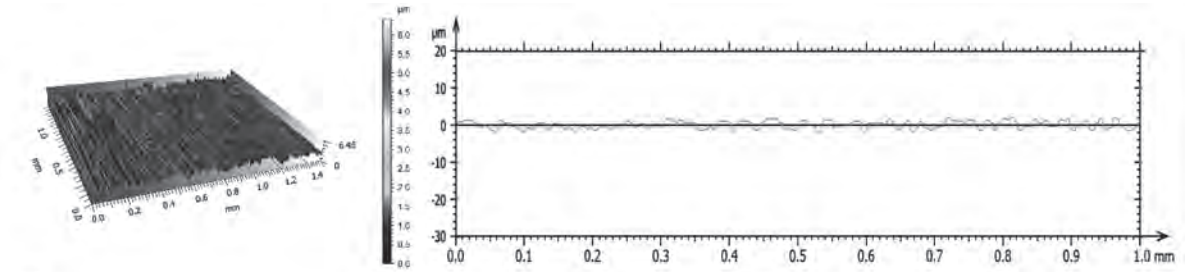

a)

Maximum depth 2.24 µm

Wear area None

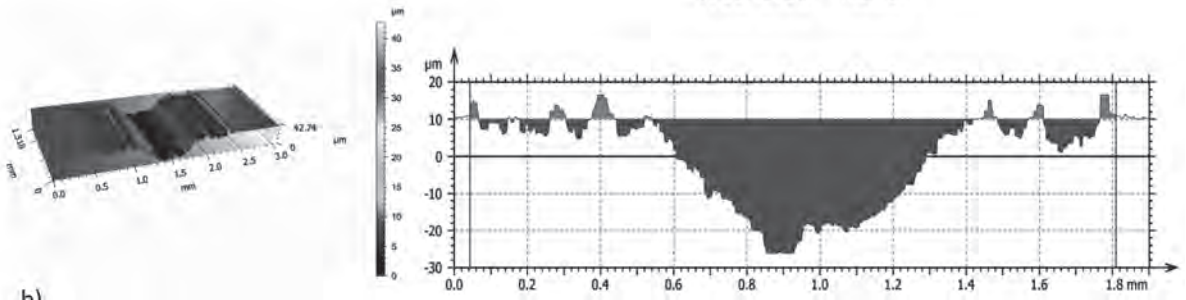

b)

Maximum depth 36.62 µm

Wear area 20630 µm^2

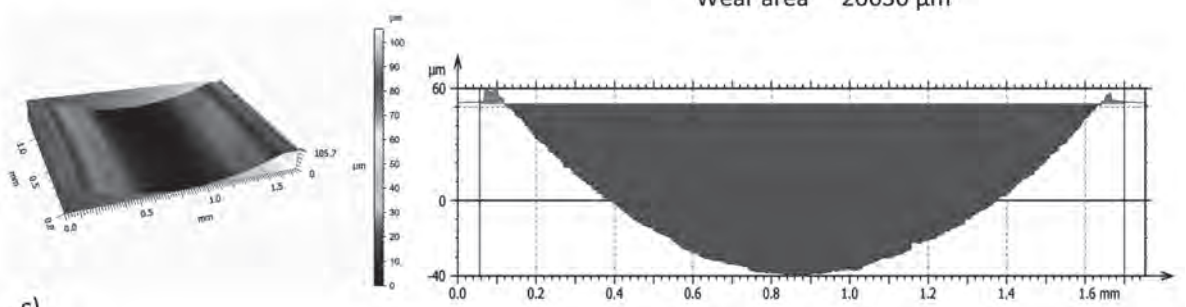

c)

Maximum depth 92.81 µm

Wear area 92339 µm^2

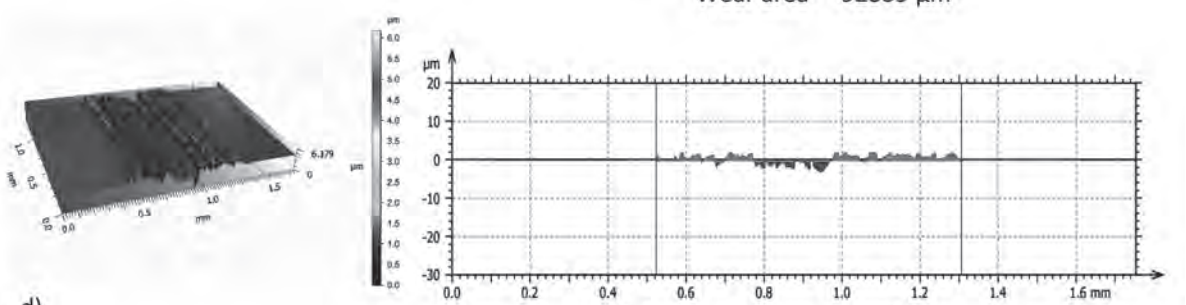

d)

Maximum depth 3.087 µm

Wear area 318.7 µm^2

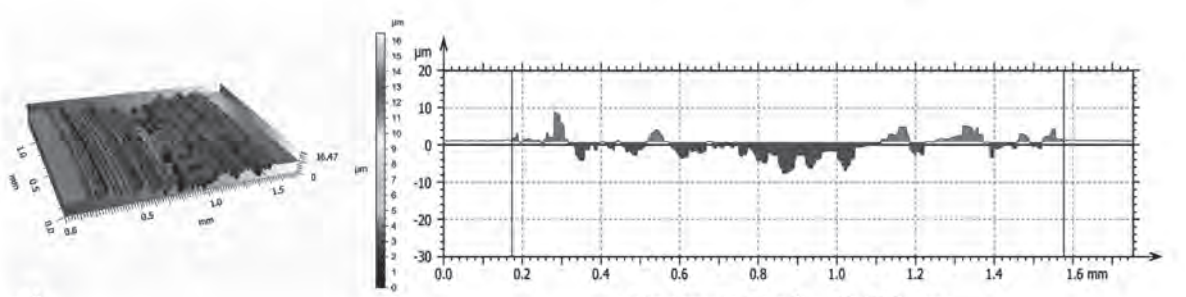

e)

Maximum depth 8.728 µm

Wear area 2685 µm^2

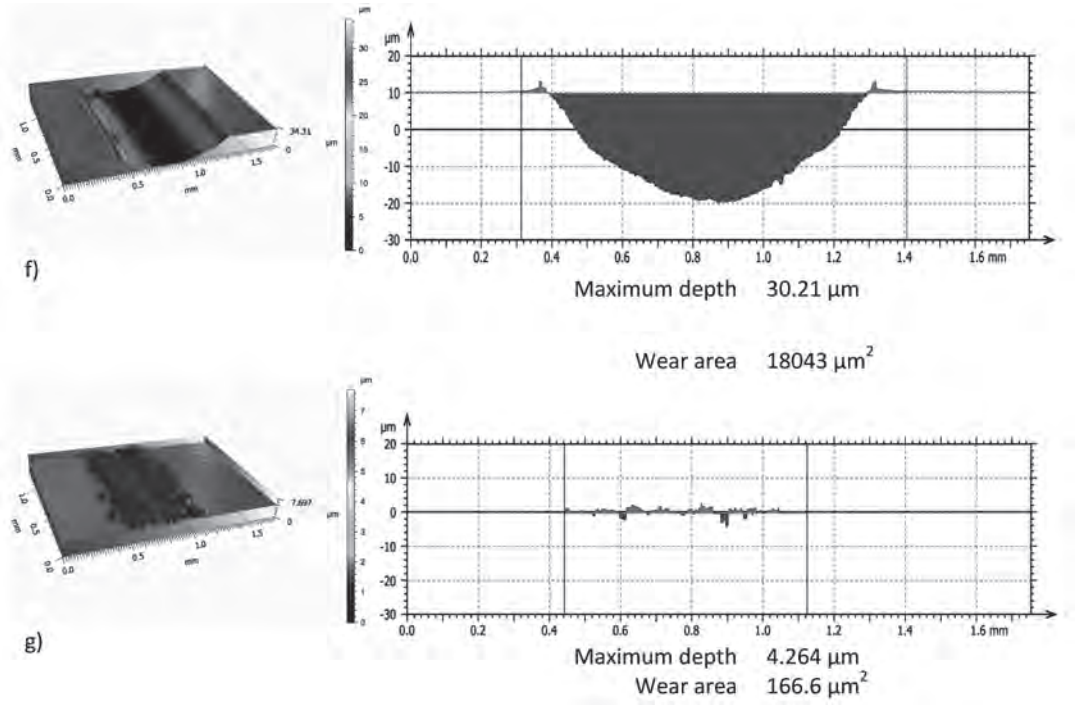

Fig. 3. The isometric image of the trace of wear and the cross-section of wear profile: a) before friction, b) 100Cr6 steel – 100Cr6 steel (load: 15 N; humidity: 50% ± 5%), c) 100Cr6 steel – Al_2O_3 (load: 15 N; humidity: 50% ± 5%), d) 100Cr6 steel – SiC (load: 15 N; humidity: 50% ± 5%), e) 100Cr6 steel – 100Cr6 steel (load: 15 N; humidity: 90% ± 5%), f) 100Cr6 steel – Al_2O_3 (load: 15 N; humidity: 90% ± 5%), g) 100Cr6 steel – SiC (load: 15 N; humidity: 90% ± 5%)

Rys. 3. Obraz izometryczny śladu zużycia i profilu wytarcia w przekroju poprzecznym dla: a) przed tarciem, b) stal 100Cr6 – stal 100Cr6 (obciążenie: 15 N; wilgotność: 50% ± 5%), c) stal 100Cr6 – Al_2O_3 (obciążenie: 15 N; wilgotność: 50% ± 5%), d) stal 100Cr6 – SiC (obciążenie: 15 N; wilgotność: 50% ± 5%), e) stal 100Cr6 – stal 100Cr6 (obciążenie: 15 N; wilgotność: 90% ± 5%), f) stal 100Cr6 – Al_2O_3 (obciążenie: 15 N; wilgotność: 90% ± 5%), g) stal 100Cr6 – SiC (obciążenie: 15 N; wilgotność: 90% ± 5%)

Table 5. Parameters of the geometric structure of the surface after the tests
Tabela 5. Parametry struktury geometrycznej powierzchni po testach

	Sq [µm]	Ssk	Sku	Sp [µm]	Sv [µm]	Sz [µm]	Sa [µm]
100Cr6 steel – 100Cr6 stel [Load: 15 N; Humidity: 50% ± 5%]	11.04	-1.442	3.587	12.74	30.00	42.74	8.674
100Cr6 steel – Al_2O_3 [Load: 15 N; Humidity: 50% ± 5%]	32.84	0.4357	1.746	65.12	40.54	105.7	28.92
100Cr6 steel – SiC [Load: 15 N; Humidity: 50% ± 5%]	0.7367	-0.7614	6.818	1.741	4.438	6.179	0.4437
100Cr6 steel – 100Cr6 steel [Load: 15 N; Humidity: 90% ± 5%]	2.437	-0.4676	4.002	8.802	7.670	16.47	1.890
100Cr6 steel – Al_2O_3 [Load: 15 N; Humidity: 90% ± 5%]	11.94	-0.465	1.495	14.48	19.82	34.31	11.16
100Cr6 steel – SiC [Load: 15 N; Humidity: 90% ± 5%]	0.6345	0.4933	8.961	2.654	5.044	7.697	0.4235

Analysis of the obtained friction coefficients at the relative humidity of 50% ± 5% and 90% ± 5% shows the running-in of the sample up to approx. 200 m of the friction path. After that, the friction coefficient stabilized. The graphs show that the coefficient of friction for all pairs tested is more stable at a relative humidity of 90% ± 5%. Linear wear of the tested surfaces decreases with a higher value of relative humidity. In this study, a correlation was observed between the friction coefficient and

the L_{Aeq} values or the emission of high-frequency sound. From the friction path of about 500 m, in the case of the 100Cr6 – 100Cr6 pair at a relative humidity of 90% ± 5%, destabilization of the friction processes is visible, characterized by cyclic high-frequency emission.

Figure 5 shows graphs of the average values of the coefficient of friction, linear wear, sound level, and wear area. The average values of friction coefficient linear wear were obtained by averaging the measurements from the tribometer. The average sound level was calculated using formula **[L. 30]**, and the wear area was defined using the formula for the volume of wear in rotational motion: $P = 2rA\pi$, where r – friction radius, A – surface area of the wear track.

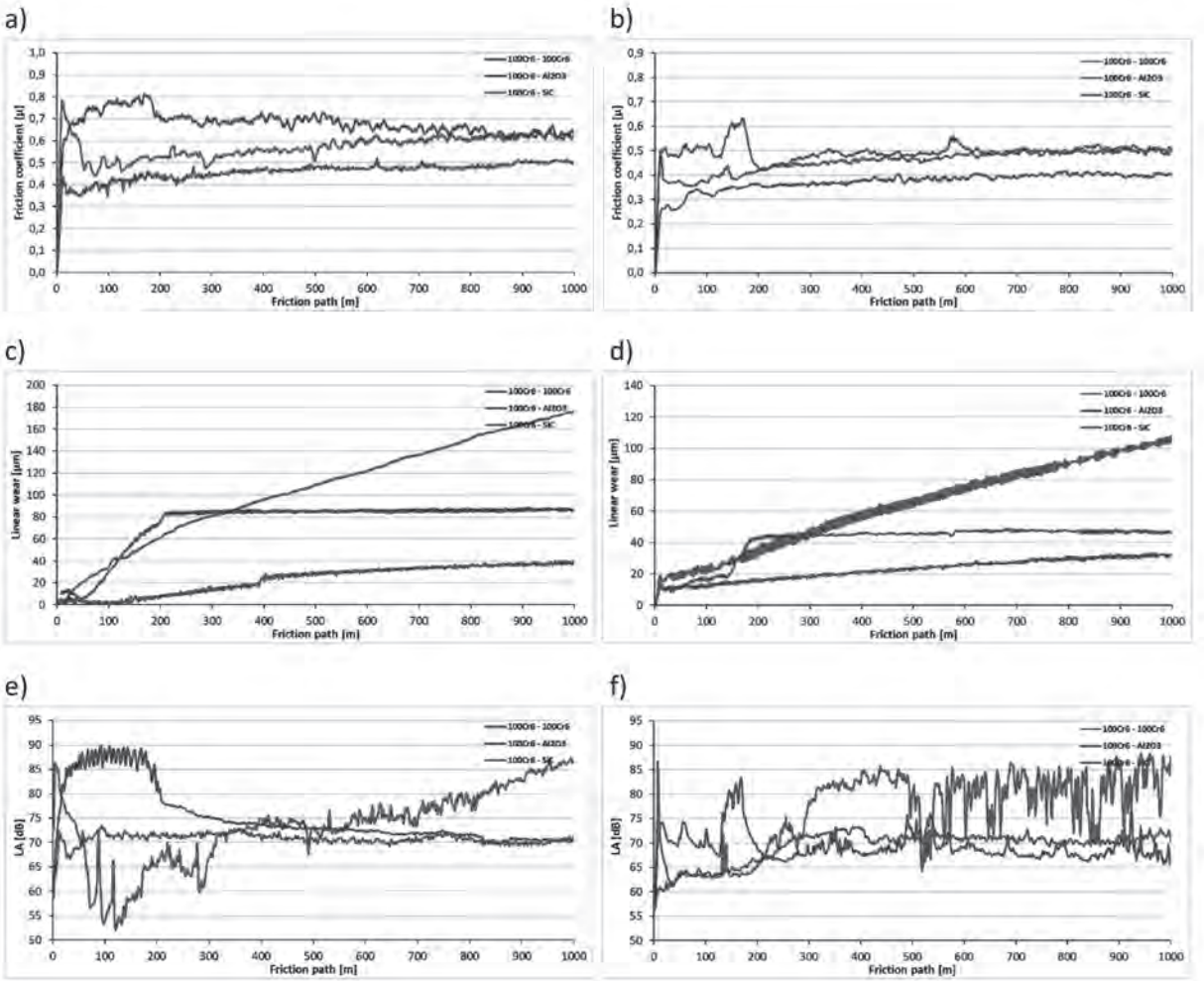

Fig. 4. Tribological and acoustic characteristics of friction configurations: a) friction coefficient (humidity: 50% ± 5%), b) friction coefficient (humidity: 90% ± 5%), c) linear wear (humidity: 50% ± 5%), d) linear wear (humidity: 90% ± 5%), e) LA values (humidity: 50% ± 5%), f) LA values (humidity: 90% ± 5%)

Rys. 4. Charakterystyki tribologiczne i akustyczne skojarzeń trących: a) współczynnik tarcia (wilgotność: 50% ± 5%), b) współczynnik tarcia (wilgotność: 90% ± 5%), c) zużycie liniowe (wilgotność: 50% ± 5%), d) zużycie liniowe (wilgotność: 90% ± 5%), e) wartości LA (wilgotność: 50% ± 5%), f) wartości LA (wilgotność: 90% ± 5%)

Analysis of the graphs in **Figure 5** shows that the lowest average values of the friction coefficient, linear wear, sound level, and wear area were obtained at a relative humidity of 90% ± 5%. The graphs indicate the highest values for the 100Cr6 – Al_2O_3 sliding pair, and the lowest for the 100Cr6 – SiC configuration. The greatest differences were found in the case of the wear area. For 100Cr6 – Al_2O_3 at a relative humidity of 90% ± 5%, the wear area was about five times smaller than under lower humidity conditions.

For the 100Cr6 – 100Cr6 pair, the wear area was more than seven and half times larger. In these pairs, the average linear wear decreased by more

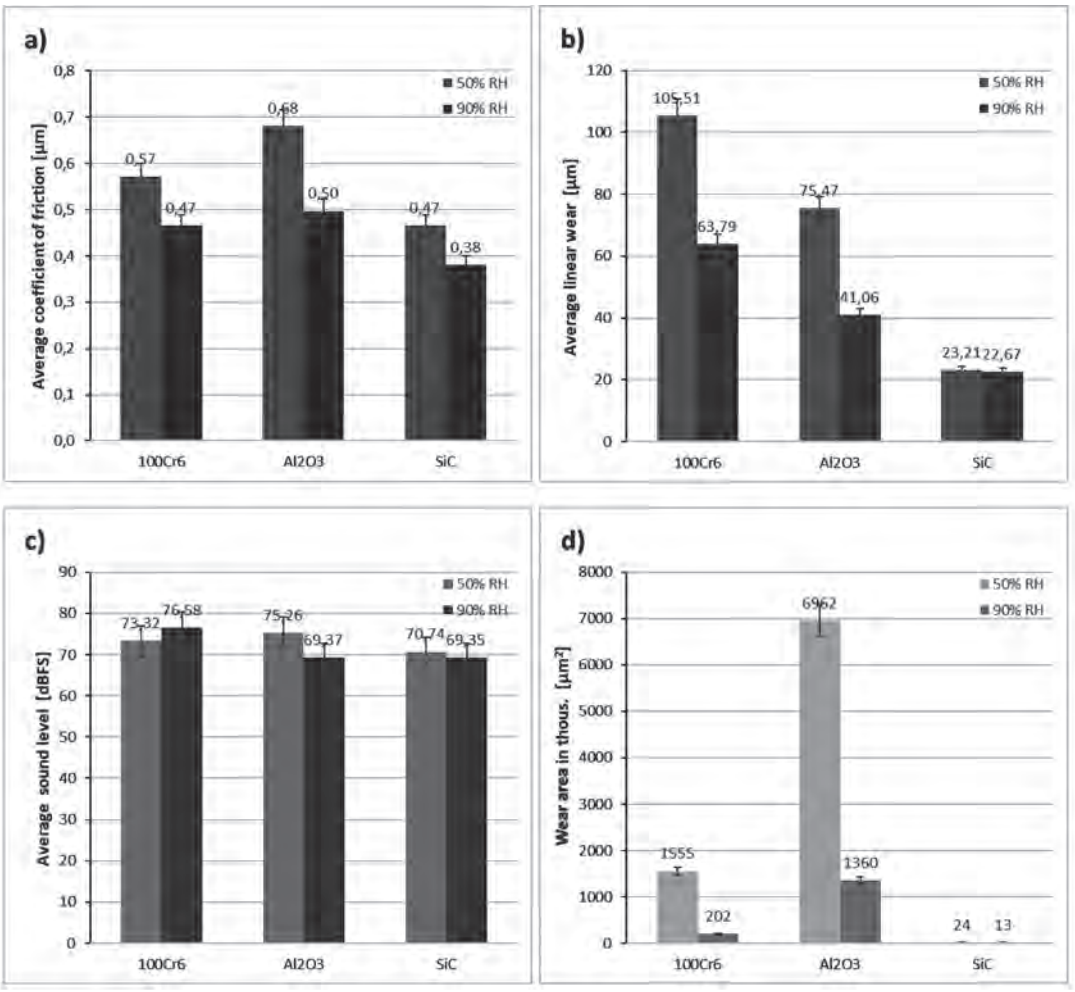

Fig. 5. Bar charts: a) average coefficient of friction, b) average linear wear, c) average sound level, d) wear area
Rys. 5. Wykresy słupkowe: a) średni współczynnik tarcia, b) średnie zużycie liniowe, c) średni poziom dźwięku, d) pola zużycia

than one and half times with increasing relative humidity. The smallest differences were observed for the 100Cr6 – SiC pair, the average linear wear, sound level, and wear area in both conditions of relative humidity are slightly lower.

CONCLUSIONS

The following conclusions were formulated based on the test results obtained:

1. The friction coefficient and linear wear were higher and the wear track was the highest for the 100Cr6 – SiC friction pair.
2. The highest value of the friction coefficient, linear wear, and the widest wear area were observed for the 100Cr6 – Al_2O_3 friction pair.
3. Due to increased relative humidity, the friction coefficient and linear wear decrease.
4. The sound level is closely related to the performance of the tribological system. Moreover, increasing relative humidity reduces the sound level, in particular, at the stage of the system running-in.
5. For the elements made of 100Cr6 steel at the running-in stage, an opposite phenomenon was observed; first the sound level increased to decrease after the running-in stage.

Acknowledgments: The authors acknowledge support from Prof. Dariusz Ozimina for providing the technical, substantive, and editorial support.

REFERENCES

1. Ozimina D., Madej M., Bugajska A., Witaszek K., Płaza S., Ozimina E., Kałdoński T.: Triboelectric phenomena during friction with diamond-like carbon coatings. "Tribologia" 2014, 6, pp. 113.
2. Ozimina D., Madej M., Desaniuk T., Żółty M., Kulczycki A.: Wpływ smaru wzbogaconego grafenem na działanie systemu tribosystem, Transakcje DEStech, 2019.
3. Chen Z., He X., Xiao C., Kim S.H.: Effect of Humidity on Friction and Wear – A Critical Review, "Lubricants" 2018, 6, pp. 74.
4. Kato K., Adachi K.: Wear of advanced ceramics. "Wear" 2002, 253, pp. 1097–1104.
5. Fischer T. E., Zhu Z., Kim H., Shin D.S.: Genesis and role of wear debris in sliding wear of ceramics, "Wear" 2000, pp. 53–60.
6. Xu J. G., Kato K.: Formation of tribochemical layer of ceramics sliding in water and its role for low friction, "Wear" 2000, 245, pp. 61–75.
7. Fischer T.E.: Friction and wear of ceramics, "Scr. Metall. Mater." 1990, 24, pp. 833–838.
8. Erdemir A., Erck R., Fenske G., Hong H.: Solid/liquid lubrication of ceramics at elevated temperatures, "Wear" 1997, 203, pp. 588–595.
9. Basu B., Vitchev R.G., Vleugels J., Celis J.P., van der Biest O.: Influence of humidity on the fretting wear of self-mated tetragonal zirconia ceramics, "Acta Mater." 2000, 48, pp. 2461–2471.
10. Murthy V. S. R., Kobayashi H., Tsurekawa S., Tamari N., Watanabe T., Kato K.: Influence of humidity and doping elements on the friction and wear of SiC in unlubricated sliding, "Tribol. Int." 2004, 37, pp. 353–364.
11. Wäsche R., Klaffke D., Troczynski T.: Tribological performance of SiC and TiB_2 against SiC and Al_2O_3 at low sliding speeds, "Wear" 2004, 256, pp. 695–704.
12. Komvopoulos K., Li H.: The effect of tribofilm formation and humidity on the friction and wear properties of ceramic materials, "J. Tribol." 1992, 114, pp. 131–140.
13. De Baets P., Kalacska G., Strijckmans K., van de Velde F., Van Peteghem A. P.: Experimental study by means of thin layer activation of the humidity influence on the fretting wear of steel surfaces, "Wear" 1998, 216, pp. 131–137.
14. Bregliozzi G., Di Schino A., Kenny J. M., Haefke H.: The influence of atmospheric humidity and grain size on the friction and wear of AISI 304 austenitic stainless steel, "Mater. Lett." 2003, 57, pp. 4505–4508.
15. Wang Y., Lei T. Q., Liu J. J.: Tribo-metallographic behavior of high carbon steels in dry sliding: I. Wear mechanisms and their transition, "Wear" 1999, 231, pp. 1–11.
16. Goto H., Amamoto Y.: Effect of varying load on wear resistance of carbon steel under unlubricated conditions, "Wear" 2003, 254, pp. 1256–1266.
17. Ferrer C., Salas F., Pascual M., Orozco J.: Discrete acoustic emission waves during stick-slip friction between steel samples.,"Tribology International 2009, 43, pp. 1–6.
18. Pau M.: Estimation of real contact area in a wheel-rail system by means of ultrasonic waves, "Tribology International" 2003, 36, pp. 687–690.
19. Eguchi M., Yamamoto T.: Shear characteristics of a boundary film for a paper – based wet friction material: friction and real contact area measurement, "Tribology International" 2005, 38, pp. 327–335.
20. Sun J., Wood R.J.K., Care I., Powrie H.E.G.: Wear monitoring by acoustic emission(AE) and electrostatic (ES) technologies, IMECHE2003.
21. Kalogiannakis G., Quintelier J., Et al.: Identification of wear mechanisms of glass/polyester composites by means of acoustic emission, "Wear" 2008, 264, pp. 235–244.
22. Douglas R. M., Steel J. A., Reuben R. L.: A study of the tribological behaviour of piston ring/cylinder liner interaction in diesel engines using acoustic emission, "Tribology International" 2006, 39, pp. 1634–1642.
23. Thompson B.D., Young R.P., Lockner D.A.: Observations of premonitory acoustic emission and slip nucleation during a stick slip experiment in smooth faulted Westerly granite, "Geophys. Res. Lett." 2005, 32, p. 10304.

24. Schubnel A., Walker E., Thompson B.D. et al.: Transient creep, aseismic damage and slow failure in Carrara marble deformed across the brittle-ductile transition, "Geophys. Res. Lett." 2006, 33, p. 17301.
25. Atkinson B.: Earthquake prediction, "Phys. Technol." 1981, 12.
26. Bureau L., Baumberger T., Caroli Ch., Ronsin O.: Low velocity friction between macroscopic solids, "Comptes Rendus de l'Académie des Sciences – Series IV – Physics" 2001, 2, pp. 699–707.
27. Kekez M., Desaniuk T., Duszczyk J., Ozimina D.: On the use of acoustic emission to assess the wear in a tribosystem, "Journal of Machine Construction" 2019, 113, pp. 99–103.
28. International Electrotechnical Commission: Electroacoustics – Sound level meters – Part 1: Specifications, IEC 61672-1:2003, IEC, 2003.
29. International Electrotechnical Commission: Audio and audiovisual equipment – Digital audio parts – Basic measurement methods of audio characteristics – Part 3: Professional use, IEC 61606-3:2008. IEC, 2008.
30. ISO 9612:2009, Acoustics – Determination of occupational noise exposure – Engineering method.